Single-scattering cluster calculations and Fourier-transform analyses of normal photoelectron diffraction

P. J. Orders and C. S. Fadley
Department of Chemistry, University of Hawaii, 2545 The Mall, Honolulu, Hawaii 96822
(Received 21 June 1982)

The results of single-scattering cluster (SSC) calculations of normal photoelectron diffraction (NPD) from the S 1*s* level in $c(2\times2)$S on Ni(001) are compared with multiple-scattering (MS) calculations by Tong and co-workers over the energy range 100 to 600 eV. It is found that the kinematical $\chi(E)$ curves are in good agreement with the multiple-scattering curves over the energy range $\sim$160 to $\sim$400 eV but in poor agreement elsewhere. The range of agreement between the SSC and MS curves can be directly associated with a relatively strong peak in the backscattering amplitude over essentially the same 160- to 400-eV range. The SSC curve for an adsorbate vertical height of $z=1.35$ Å is also in good agreement with experimental data of Hussain and co-workers over the range of $\sim$170—430 eV. Thus, it appears that this simple SSC model can be fruitfully used in analyzing NPD data, even if it may not be quantitative enough for refined structural determinations. The effects of cluster size are examined within the single-scattering model, and it is suggested that approximately eight Ni layers are needed to describe NPD at electron energies $\gtrsim$300 eV. Inclusion of instrumental angular broadening is also found to be significant, and in particular increases the agreement between SSC and MS curves. Fourier-transform analysis of both the single- and multiple-scattering curves shows that peaks in the magnitude of the Fourier transform are most directly related to path-length differences between the direct wave and various scattered waves and *not* to perpendicular interlayer distances as previously suggested. These results thus indicate that the Fourier transformation of normal photoelectron diffraction data is not a particularly reliable method of obtaining surface structural information unless a very limited number of path-length differences are strongly predominant in the scattering.

I. INTRODUCTION

Normal photoelectron diffraction (NPD) has been shown to have considerable promise as a technique for structural analyses of adsorbate bonding on single-crystal surfaces.[1–5] Deriving structures by this method in the most accurate way, however, involves fitting the results of multiple-scattering calculations performed at various adsorbate sites and at various adsorbate-substrate distances to the experimental data, exactly as in low-energy-electron diffraction (LEED). Thus the technique is encumbered somewhat by the need to perform numerous multiple-scattering calculations in order to fit the experimental data and eliminate unlikely adsorption sites. In several recent studies, however, it has been shown that Fourier transforms of both multiple-scattering theoretical curves[5] and experimental data[3] exhibit peak positions in the magnitude of the Fourier transform that are closely related to certain perpendicular interlayer distances, thus hopefully providing a more direct and simple method of structural analysis.

If the peaks in the magnitude of the Fourier transform are simply related to perpendicular interlayer distances, prior experience with the analysis of extended x-ray-absorption fine-structure (EXAFS) data[6] thus strongly suggests that some form of single backscattering from the underlying layers must be the dominant mechanism producing photoelectron diffraction. Hence one might expect that a simple kinematical theory would provide a good description of at least certain aspects of NPD. We have thus applied such a single-scattering or kinematical model to the analysis of NPD from the S 1*s* core level of $c(2\times2)$S on Ni(001) over the rather broad electron kinetic energy range from 100 to 600 eV. The system $c(2\times2)$S on Ni(001) was chosen because its structure has been very well defined in prior studies by different techniques[3,7,8] and also because of the availability of comprehensive experimental NPD data[9] over an extended data range, as well as comparative multiple-scattering calculations[10] over an essentially equivalent energy range from $\sim$110 to 610 eV. Although it is clear from the outset that properly executed multiple-scattering calculations will better describe NPD results than equivalent single-scattering calculations, the extreme

complexity of the multiple-scattering theory and hence the long computation times required make it useful to explore the degree to which a much simpler approach can be utilized. Also, a decided advantage of the kinematical model is that a given calculation can be much more easily dissected so as to estimate which atoms contribute as the strongest scatterers, what their corresponding scattering amplitudes and angles are, and how their phases relate to one another. This type of analysis proves to be especially useful in fully understanding both single- and multiple-scattering NPD curves and their Fourier transforms.

The single-scattering cluster (SSC) model to be used here is described in Sec. II. The results of single-scattering calculations are compared with those of multiple-scattering calculations and with experimental results in Sec. III as both intensity versus energy curves and Fourier transforms. Section III also includes a detailed analysis of the Fourier-transform results. The conclusions drawn from these comparisons are presented in Sec. IV.

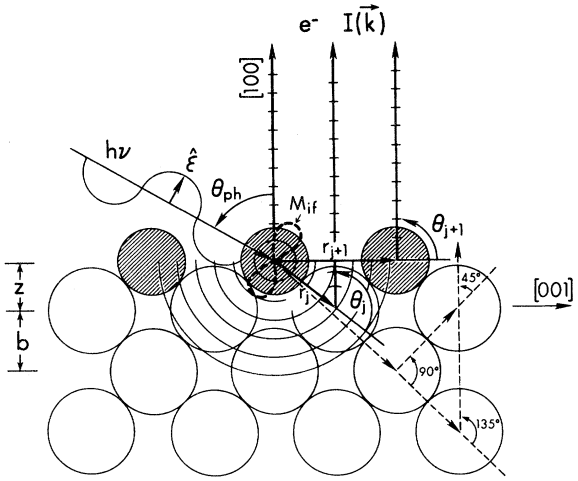

FIG. 1. Schematic illustration of the geometry employed in SSC calculations of normal photoelectron diffraction. The index j represents single scattering from a typical substrate atom, whereas $j+1$ represents adsorbate single scattering. The dashed lines at lower right show possible substrate multiple-scattering events not included in the model.

II. SINGLE-SCATTERING CLUSTER CALCULATIONS

The SSC model we have employed is essentially the same as that described by Kono *et al.*[11] for determining adsorbate geometries from azimuthally scanned x-ray photoelectron diffraction (XPD) data. This model has recently been further tested in comparisons to XPD data for S and Se on Ni(001) and found to provide a very good description of such high-energy ($\sim 10^3$ eV) photoelectron diffraction phenomena.[12] The overall wave amplitude producing emission into a given direction is represented as the summation of the primary (or unscattered) wave as excited from a core level of an adsorbate atom in a finite cluster with those waves that are scattered once by all other substrate and adsorbate atoms in the cluster. The physical geometry is shown schematically in Fig. 1. Such a kinematical description of an NPD experiment requires, however, several changes to the model as previously used for azimuthal XPD. These are the following: (1) The integration with respect to the photon polarization vector $\hat{\epsilon}$ is removed so as to account for the polarized nature of the synchrotron radiation used in the NPD experiment; (2) as photon energy is swept in the NPD experiment, an energy dependence must be included in a number of parameters, and this is most conveniently written as a dependence on photoelectron wave vector k for the relevant quantities in equations to be presented below; and finally (3) a phase shift Φ (equal to 0° for emission from p and f subshells and 180° for emission from s and d subshells) is included in order to describe the possible phase shift between the primary and scattered waves caused by the parity of the dipole-excited photoelectron wave.[9,13] A further important physical difference in NPD to be noted is that it is predominantly backscattering events with scattering angles $\theta_j \approx 180°$ that should predominate, whereas in azimuthal XPD at $\sim 10^3$ eV, the strong forward scattering dominance in the scattering factor will cause events for $\theta_j \approx 0°$ to be the most important.

These changes to the XPD single-scattering cluster model[11] yield the following general starting equations for describing emission into the $\vec{k}$ direction in the NPD experiment:

$$I(\vec{k}) \propto \left| (\hat{\epsilon}\cdot\hat{k})e^{-\gamma(k)L} + \sum_j \frac{\hat{\epsilon}\cdot\hat{r}_j}{r_j} f_j(\theta_j,k) W_j(\theta_j,k) e^{-\gamma(k)L_j} \exp[ikr_j(1-\cos\theta_j)+\Phi] \right|^2$$

$$+ \sum_j (\hat{\epsilon}\cdot\hat{r}_j)^2 \frac{|f_j(\theta_j,k)|^2}{r_j^2} [1-W_j(\theta_j,k)^2] e^{-2\gamma(k)L_j} , \quad (1)$$

where $\hat{\epsilon}\cdot\hat{k}$ and $\hat{\epsilon}\cdot\hat{r}_j$ represent the polarization dependence of the primary excitation matrix elements (here $1s\rightarrow p$ wave); $e^{-\gamma(k)L}$ and $e^{-\gamma(k)L_j}$ represent the effects of inelastic scattering on primary and scattered waves traveling distances of L and L_j, respectively; $\gamma(k)=1/2\Lambda_e(k)$ if Λ_e is the usual electron mean free path; $f_j(\theta_j,k)$ is an energy-dependent complex scattering factor equal to $|f_j(\theta_j,k)|\exp[i\psi_j(\theta_j,k)]$; $W_j(\theta_j,k)$ is an energy-dependent Debye-Waller factor equal to $\exp[-2k^2(1-\cos\theta_j)\bar{U}_j^2]$; $\bar{U}_j^2$ is the one-dimensional mean-squared displacement of the jth atom with respect to the emitter, $kr_j(1-\cos\theta_j)$ is the phase shift introduced by the path-length difference between the primary wave and the jth scattered wave, and the second summation term represents the contribution to the intensity from thermal diffuse scattering (TDS). Any energy dependence in the primary photoionization cross section has been omitted.

The energy dependence of the electron attenuation terms through $\Lambda_e(k)$ was approximated by assuming a Λ_e in Ni that is proportional to (kinetic energy)$^{1/2}$, having a minimum value of 3.5 Å at 80 eV and a value of 9.5 Å at 600 eV. These values are thus consistent with a recent tabulation of Λ_e data for various materials,[14] especially those quoted for Ni. The mean free path in the overlayer was assumed to be twice that of the bulk value due to its lower atomic density. The complex scattering factors $f_j(\theta_j,k)$ for S and Ni were determined via a LEED-type partial-wave method and a program MUFFPOT provided to us by J. B. Pendry. The S and Ni partial-wave phase shifts (which ranged from a minimum number of 10 to a maximum of 20 as the electron kinetic energy was increased from 100 to 600 eV in 5-eV increments) were obtained from a muffin-tin potential for an atomic crystal simulating the S overlayer on Ni(001) and for an fcc Ni crystal, respectively. The remaining energy-dependent term, the magnitude of the electron wave vector k, is simply related to the electron kinetic energy E (equal to $h\nu$ minus binding energy) by the free-electron dispersion relationship $k=(2mE)^{1/2}/\hbar$, and unless otherwise specified we will consider all kinetic energies to be measured *inside* the crystal. Thus for most of our discussion, no V_0 corrections are involved.

The above equation can be further simplified in a straightforward way so as to elucidate the dominant terms producing the intensity modulations with energy. The TDS summation will show only slow and rather smooth variation with energy through a complicated sum involving f_j, W_j, and γ and so can be discarded as a significant source of the NPD oscillations. Equation (1) can then be conveniently rewritten as

$$I(\vec{k})\propto\left|A_0+\sum_j A_j(k)\exp[i\arg_j(k)]\right|^2, \tag{2}$$

where

$$A_0=(\hat{\epsilon}\cdot\hat{k})\exp[-\gamma(k)L],$$

$$A_j(k)=\hat{\epsilon}\cdot\hat{r}_j\frac{|f_j(\theta_j,k)|}{r_j}W_j(\theta_j,k)e^{-\gamma(k)L_j},$$

and

$$\arg_j(k)=kr_j(1-\cos\theta_j)+\psi_j(\theta_j,k)+\Phi.$$

Note that the overall scattering phase shift ψ_j is now included in $\arg_j(k)$. Also, in general, it may be convenient to include a factor N_j in A_j to allow for summing over a set of symmetry-equivalent atoms with the same r_j and θ_j. We can now expand Eq. (2) to give

$$I(\vec{k})\propto A_0^2+2A_0\sum_j A_j(k)\cos[\arg_j(k)]+\left[\sum_j A_j(k)\exp\{i[\arg_j(k)]\}\right]\left[\sum_j A_j(k)\exp\{-i[\arg_j(k)]\}\right]. \tag{3}$$

Now we shall assume the A_j's to be at least an order of magnitude less than A_0 over the energy range 100 to 600 eV, so that the product of the cross terms can be neglected. This yields the following simplified EXAFS-type expressions for the fractional photoelectron intensity modulation as a function of energy:

$$\chi(E)=\frac{I(k)-I_0}{I_0}\propto 2\sum_j\frac{A_j(k)}{A_0}\cos[\arg_j(k)], \tag{4}$$

or with $\arg_j(k)$ written out in full,

$$\chi(E)\propto 2\sum_j\frac{A_j(k)}{A_0}\cos[kr_j(1-\cos\theta_j)+\psi_j(\theta_j,k)+\Phi]. \tag{5}$$

Because A_0 and Φ are constants and $A_j(k)$ and $\psi_j(\theta_j,k)$ are slowly varying functions of energy, the intensity modulations are thus predicted in this model to be primarily produced by the energy-dependent phase shift due to path-length difference

or $kr_j(1-\cos\theta_j)$. Equations (4) or (5) can also be considered as $\chi(k)$ curves and Fourier transformed to yield peaks of varying strengths $\propto A_j/A_0$ and positions given by $r_j(1-\cos\theta_j)$, rather than at twice the interplanar distance from the adsorbate to a given substrate layer as suggested in prior NPD analyses.[5,13,15]

Two different atomic clusters were used in the calculations. The first consisted of a $c(2\times2)$ overlayer of S atoms in fourfold hollow sites together with eight underlying layers of Ni atoms totaling 1884 atoms. The second cluster had the same S overlayer but only four Ni layers with a total of 1029 atoms. The mirror symmetry about the [001] direction introduced by the chosen NPD experimental geometry[9] was further used to reduce the actual size of the cluster in the calculations to approximately half that of the stated total number of atoms. Various trial calculations with different cluster sizes verified that the sizes quoted were fully converged as to directions parallel to the surface; the eight-layer cluster was also found to be converged as to direction into the substrate. In fact, the sizes quoted are rather conservative, as it is usually $\lesssim 200$ atoms that are found to produce most of the NPD modulation.

Calculations were performed with no instrumental angular broadening as well as with broadening due to a 3° half-angle acceptance aperture.[9] The latter was included by summing over a nine-point mesh centered on a circle of 4° diameter, with one point at the center and eight points equally spaced on the periphery.

III. RESULTS AND DISCUSSION

A. Theoretical $\chi(E)$ curves

The solid and dotted $\chi(E)$ curves shown in Fig. 2 represent the normalized photoelectron intensity modulation from the S 1s core level (for which the final-state parity yields $\Phi=180°$) for $c(2\times2)$S on Ni(001) as predicted by the SSC model. The curves are presented as a function of the S 1s electron kinetic energy inside the solid for values between 100 and 600 eV. The calculations were performed at z distances of 1.213, 1.407, 1.602, and 1.796 Å above the Ni surface, with the S atoms occupying the fourfold hollow sites and the photon incidence direction fixed at a polar angle of $\theta_{ph}=60°$ with respect to the surface normal and lying in the plane containing the [100] and [001] directions. The solid curves represent the results of single-scattering calculations on a larger eight-layer atomic cluster (989 atoms total consisting of 65 S atoms and 924 Ni atoms) and the dotted curves represent the results of the same calculation on a smaller four-layer atomic cluster

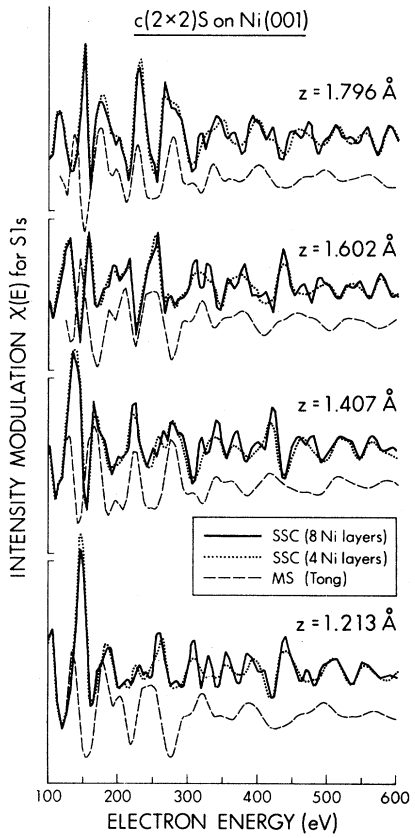

FIG. 2. Comparison of single-scattering cluster model $\chi(E)$ curves with multiple-scattering curves due to Tong *et al.*[10] for four z positions of $c(2\times2)$S on Ni (001) in fourfold hollow sites. The solid curves represent the SSC results obtained from a cluster containing eight Ni layers and the dotted curves SSC results from a cluster containing four Ni layers.

(527 atoms total consisting of 65 S atoms and 462 Ni atoms). Both calculations neglect the effects of instrumental angular broadening. The dashed curves are the results of multiple-scattering calculations performed by Tong and co-workers[10] over the energy range 110 to 610 eV (again measured inside the solid) with the same z distances and photon incidence-electron emission geometry as that used in the single-scattering calculations. The multiple-scattering (MS) calculations used a substrate thickness of four atomic layers. The MS curves have been vertically offset from the corresponding single-scattering curves for clarity; however, the intensity scales are the same for all curves shown. The magnitudes of the oscillations in all curves decrease from typical values of 60% of I_0 at low energies ($\sim$150 eV) to 15% of I_0 at energies around 500 eV, principally due to the damping effects of the energy-dependent Debye-Waller factors.

Because the multiple-scattering calculations have

been terminated at the fourth Ni layer, the most correct comparisons of the two theories should be made with the results of the four-layer single-scattering calculations (dotted curves). However, before making such comparisons we turn briefly to the effects of cluster size on the results of the single-scattering calculations. It can be seen that for electron energies $\lesssim 300$ eV, the solid and dotted curves representing the eight- and four-layer clusters, respectively, are essentially equivalent for all z values, while for energies $\gtrsim 300$ eV more appreciable differences begin to be observed, with more fine structure present in the eight-layer curves. In particular, the frequencies of the oscillations in the eight-layer curves are significantly greater than those in the corresponding four-layer curves. These differences can be qualitatively attributed to the energy dependence of the electron mean free path, which will at lower energies of $\lesssim 250$ eV tend to favor atoms very near the surface for both four- and eight-layer calculations. For higher energies, however, appreciable backscattering is possible from atoms deeper within the substrate, and it is these atoms with larger r_j values that will contribute higher frequencies to the $\chi(E)$ curves [cf. Eq. (5)]. This clearly shows that the four-layer single-scattering calculations have not converged as to cluster size and thus raises the question as to whether the multiple-scattering calculations[10] in their present four-layer form can give a fully accurate description of the NPD experiment at higher energies. To be sure, multiple-scattering events may tend to diminish the differences found between results for large and small clusters, but this uncertainty needs to be resolved, especially as experimental NPD data is now becoming available for comparisons over extended energy ranges.[9]

Turning now to a comparison of the four-layer single-scattering curves with the corresponding multiple-scattering curves yields surprisingly good agreement, particularly over the energy range from ~ 160 to ~ 400 eV and for the three highest z values. Table I contains the energy positions of the peaks for all of the calculations and for all four z values. We will begin by comparing the unbroadened four-layer single-scattering results [column labeled SSC-4 Ni, (a)] with those of the multiple-scattering calculation. The comparison at $z=1.213$ Å over the energy range 160–400 eV yields the worst agreement of the four cases studied. For this z value, the maximum energy difference $\Delta E_{\max}$ is found to be 12 eV for the multiple-scattering peak at 248 eV while the positions of the other peaks differ by amounts ranging from 3 to 10 eV, thus resulting in an average energy shift ΔE_{av} of 7 eV. Making similar comparisons for the remaining z positions over the energy range 160–400 eV, we find rather good agreement between the results of the two calculations for both the relative intensities of individual features and their energy positions. At $z=1.407$ Å, $\Delta E_{\max}=7$ eV for the multiple-scattering peak at 360 eV and ΔE_{av} is 3 eV. At $z=1.602$ Å, $\Delta E_{\max}=7$ eV for the multiple-scattering peak at 185 eV and $\Delta E_{\text{av}}=5$ eV. At $z=1.796$ Å, $\Delta E_{\max}=5$ eV for the multiple-scattering peaks at 195, 225, and 335 eV and $\Delta E_{\text{av}}=4$ eV. There are a few instances, typically two for each z position, where a weak feature in the multiple-scattering curve does not have a counterpart in the single-scattering data and/or vice versa. Such discrepancies, however, do not significantly affect the overall conclusion that good agreement is obtained in this energy range. At energies less than 160 eV systematic and appreciable differences are observed between the results of the two calculations, but this is not surprising inasmuch as for energies $\lesssim 100$ eV one surely expects multiple-scattering effects to be very strong. For example, the single-scattering calculation predicts the peak in this range to lie approximately 12 eV above its multiple-scattering counterpart for all four z positions. At energies greater than 400 eV the agreement between SSC and MS again begins to deteriorate for each z. ΔE values increase to typically 15 eV and it becomes increasingly more difficult to determine the corresponding features between the multiple- and single-scattering curves. Some peaks in the multiple-scattering curves actually occur at positions of minima in the single-scattering data.

It remains then to explain more quantitatively the origin of this behavior: the disagreement between single- and multiple-scattering at low-electron energies, the good agreement in the energy range from ~ 160 to ~ 400 eV, and finally the poor agreement again at energies $\gtrsim 400$ eV. In doing this, it is useful to consider the strength of the backscattering amplitude $|f(180°)|$, especially as measured relative to that at scattering angles not too far from backscattering. Figure 3 thus shows the ratio of the backscattering amplitude to the amplitude at scattering angles of 0°, 45°, 90°, and 135° for Ni as a function of electron kinetic energy between 30 and 600 eV. As expected, these ratios show that, over the entire energy range, the amplitude of the scattering factor is peaked in the forward ($\theta_j=0°$) and backward ($\theta_j=180°$) directions. More interestingly, a very strong peak in the ratio $|f(180°)|/|f(135°)|$ is seen over the energy range of ~ 100–350 eV. That is, the scattering amplitude is much more strongly peaked in the backward direction over these energies, a fact which may directly explain the better agreement found between

TABLE I. Comparison of theoretical NPD $\chi(E)$ peak positions for $c(2\times2)$S on Ni(001) at four different vertical distances for four single-scattering cluster calculations and multiple-scattering (MS) calculations (Ref. 10). The columns labeled (a) represent unbroadened data and those labeled (b) represent data including a ±3° angular broadening to simulate instrumental effects. Numbers labeled with (w) indicate weak features in the $\chi(E)$ curves.

SSC-8Ni (eV)		SSC-4Ni (eV)		MS-4Ni (eV)	SSC-8Ni (eV)		SSC-4Ni (eV)		MS-4Ni (eV)
(a)	(b)	(a)	(b)	(Tong)	(a)	(b)	(a)	(b)	(Tong)
		$z=1.213$ Å					$z=1.407$ Å		
147	147	147	147	136	137	137	138	138	126
187	185	183	183	180	165	165	168	168	165
				205	223	225	222	227	223
230	240	227			250(w)	245(w)			
							260		
258	257	260	255	248	265(w)				
308	305	310	305	300(w)	272	278	278	275	275
330	330			323	320	318			
							337		337
355	356	355	350	350(w)	342	342		350	
387	387	395	393	387	370	368	367		360
408(w)	400(w)				400				
						412	418	412	415
440	445	440	442		422				
470				460(w)	458	455			
							465	468	
505	510	510	505	496	478	478			
552	550	555	553	570	525	522	525	522	513
					565	570	563	568	585
		$z=1.602$ Å					$z=1.796$ Å		
130	128	127	125	120	115	115	113	115	
155	158	155	158	145	149	150	149	148	135
193	192	192	190	185	173	177	175	175	173
215	210	213	207	210	200(w)	200(w)	200(w)	200(w)	195(w)
255	255	250	250	247	228	230	230	232	225
308	305			295(w)	275	273	275	275	275
		315	308						
327	327			320	318	315(w)	330(w)		
355	355			355(w)	340	340	348	340	335
		370	380						
380(w)	380			375	363	365(w)			
410(w)					390				
						400	398	402	400
435	435	437	432		418				
464	463			455	447	448			
							460	453	470(w)
490	490	495	488		470	470			
525					510	505	512	505	495
	530	535	535	530					
545					555	540	552	545	556
575	585	575	585		587		588		

single- and multiple-scattering calculations over a similar energy range. To expand upon this, in an NPD experiment on a (001) face of an fcc crystal, some important multiple-scattering angles are 0°, 45°, 90°, and 135° (cf. the dashed arrows in Fig. 1). The ratios plotted in Fig. 3 show that scattering in these preferred directions occurs with a much reduced amplitude to that in the backward direction,

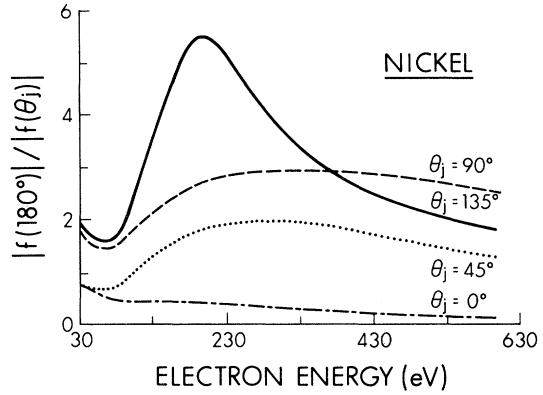

FIG. 3. Plot of the electron-energy dependence of the ratio of the amplitude of the Ni scattering factor in the backward direction $\theta_j = 180°$ with the amplitude of the scattering factor in the directions $\theta_j = 0°$, 45°, 90°, and 135°.

particularly in the energy range 160—400 eV where the backscattering amplitude reaches values 5.5 times greater than that at 135° and 3.0 times greater than that at 90°. Although the amplitude for scattering through 45° is at best only a factor of 2.0 smaller than the backscattering amplitude over this energy range, in order for 45° to be important in any multiple-scattering event, it must be accompanied by one or more scattering events through larger angles $\lesssim 135°$ (cf. Fig. 1), and this would further reduce the amplitude of the resultant multiply scattered wave with respect to the singly backscattered wave. Overall then, the combination of rather direct backscattering followed by forward scattering remains the only multiple-scattering event that is expected to produce a wave of appreciable amplitude over the range of ~160—400 eV, and it does not appear to be overly important. Below ~160 eV the amplitude ratios for scattering angles of 45°, 90°, and 135° decrease to typical values of 0.8, 1.8, and 2.0, respectively, and so the kinematical model, not surprisingly, breaks down. Above ~400 eV, the relative strength of the peak in the backscattering direction decreases to such an extent that the amplitude ratios for all of the angles given except 0° become comparable to the values in the low-energy region; thus again multiple-scattering effects should become more important. This conclusion thus suggests that the acquisition of NPD data at higher energies of $\gtrsim 400$ eV may not lead to a simplification of the necessary theoretical analysis, but rather to the converse. In fact, any multiple-scattering calculations necessary would become even more complicated because of the larger number of partial-wave phase shifts needed to determine $f_j(\theta_j)$ and the larger atomic clusters needed. By contrast, a near-kinematical regime appears to exist for Ni back-

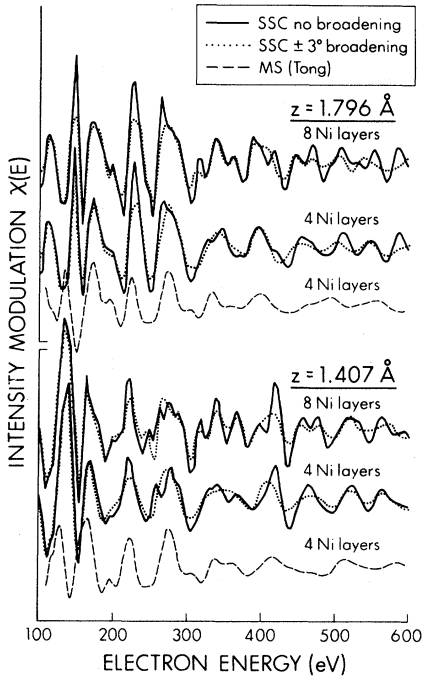

FIG. 4. Effects of angular broadening on the single-scattering cluster $\chi(E)$ curves for $c(2\times2)$S on Ni (001) at z distances of 1.407 and 1.796 Å. The solid curves are unbroadened results and the dotted curves results that include a ±3° angular broadening to simulate instrumental effects.

scattering in the intermediate range 160—400 eV, and analogous regimes would be expected for other substrates as well, but perhaps with slightly different energy ranges.

As a contrasting example, high-energy ($\sim 10^3$ eV) azimuthal x-ray photoelectron diffraction at *grazing* emission angles can be successfully described by a purely kinematical model[11,12] as the scattering is in this case dominated by the very strong peak in the amplitude of the scattering factor in the forward direction. For NPD, it is the same sort of phenomenon, that is, a relatively strong peak in $|f_j|$, but in this case in the backward direction, that allows the simple kinematical model to be such a good approximation to the more complicated dynamical model over the energy range 160—400 eV.

Figure 4 illustrates a further effect of potential importance in comparing NPD theory and experiment: the angular averaging caused by the electron analyzer. Shown here are angular broadening effects on single-scattering calculations at z positions of 1.407 and 1.796 Å. The method of including the angular broadening was discussed in the preceding section. The chosen cone of ±3° represents the acceptance angle of the analyzer used by Hussain *et al.*[9]

to obtain the NPD experimental data that will be discussed shortly. It thus represents a typical degree of angle spread in such studies. The solid curves represent the results of single-scattering calculations without instrumental broadening for both the eight- and four-layer clusters and the dotted curves the results of the same calculations with a $\pm 3°$ instrumental broadening included. Again the dashed curves are the results of the multiple-scattering calculation with no broadening. There are three notable differences introduced by the inclusion of angular broadening: (1) The amount of fine structure in both the eight- and four-layer curves is significantly reduced in the broadened data, (2) the relative amplitudes of some features have been altered and the intensity modulations at high energies have been reduced in the broadened data, and (3) a number of peaks has been shifted in energy, in some cases by as much as 10 eV in the broadened data [see Table I, columns labeled (b)]. Item (1) reduces somewhat the differences between the eight- and four-layer calculations while both items (1) and (2) improve the qualitative agreement with the multiple-scattering data across the entire energy range. Item (3), however, is not found to affect the good agreement between the SSC and MS curves in the range 160—400 eV, nor does it improve the agreement at other energies. Thus if the single-scattering calculations are used to qualitatively judge what might occur in an NPD experiment, it appears that an improvement in the structural sensitivity of the technique could be achieved by using better angular resolution. Also, these results suggest that comparing nonbroadened multiple-scattering calculations with inherently broadened experimental results may lead to erroneous structural conclusions, at least on a very fine scale of comparison. However, the fact that angle broadening somewhat improves the agreement between single- and multiple-scattering curves over the whole energy range may suggest that it effectively averages over diffraction features in a manner equivalent to the smearing of features generally associated with multiple-scattering phenomena. If the last is true it would mean that higher angular resolution may not be critical in NPD. Only the acquisition of higher-resolution experimental data and appropriately broadened multiple-scattering curves will fully resolve these points.

B. Comparison of experimental and theoretical $\chi(E)$ curves

The final arbiter of any theory is experiment, and we thus show in Fig. 5 normalized experimental $\chi(E)$ data for the S 1s level of $c(2\times2)$S on Ni(001) over the energy range ~ 100 to ~ 430 eV as obtained

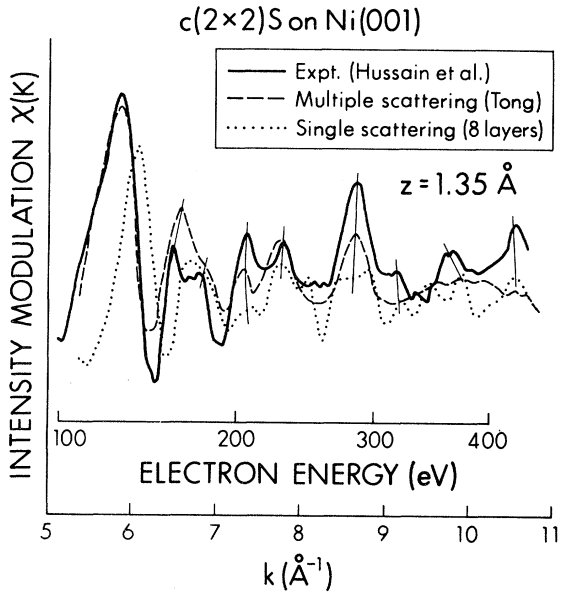

FIG. 5. Comparison of the results of single- and multiple-scattering $\chi(E)$ calculations at $z=1.35$ Å with experimental NPD data due to Hussain *et al.*[9] The single-scattering curve was obtained with a cluster containing eight Ni layers and includes a $\pm 3°$ angular broadening.

by Hussain *et al.*[9] (solid curve). Comparison with various multiple-scattering calculations has yielded the best agreement for a z value of 1.35 Å and the optimum MS results are shown as the dashed curve. The results of our single-scattering calculation at the equivalent z distance are shown as the dotted curve; these results correspond to a fully converged eight-layer cluster, with full allowance for instrumental broadening. The agreement between experiment and multiple-scattering theory is excellent over the energy region of ~ 120—300 eV, but above 300 eV, it is relatively poor with no genuine correspondence of features. This disagreement at higher energies is perhaps related to the fact that the multiple-scattering calculation was terminated at the fourth Ni layer. By contrast, the agreement between experiment and single-scattering theory is very good for all energies above ~ 170 eV with the expected disagreement being evident at lower energies. The only areas of significant deviation between the two curves at energies $\gtrsim 170$ eV are a peak at ~ 250 eV in the single-scattering curve where one does not exist in the experiment and the incorrectly predicted splitting of the experimental peak at ~ 360 eV. Overall, multiple scattering correctly predicts the positions and approximate relative intensities of six of the nine prominent features in the experimental data, whereas single scattering is almost as good for a total of seven of these at higher energies.

It remains then to comment on the general utility of single-scattering calculations in NPD. Although there is generally good agreement between the kinemetical and dynamical calculations over the energy range 160—400 eV, the few differences that do exist probably will prohibit the use of the simple theory for determining adsorbate-substrate distances with high accuracy. However, it seems very reasonable to expect the kinematical theory to be very useful in eliminating unlikely adsorption geometries (e.g., atop versus bridge sites) by making comparisons with experiment before proceeding to employ the much more laborious dynamical theory for the most likely geometries. Also, the success of the SSC model over the 160—400-eV range suggests that it could be useful in trying to understand in more detail what Fourier transforms of NPD data really mean, and this we turn to in the next section.

C. Fourier-transform of theoretical $\chi(E)$ curves

Fourier-transform (FT) analyses of the results of multiple-scattering calculations[5] and NPD experimental data[3] have suggested a simple relationship between the positions of the peaks in the magnitude of the Fourier transform and the perpendicular distances from the adsorbate to the various substrate layers below. We have further tested this idea by applying a similar analysis to the theoretical curves shown in Figs. 2 and 4. The multiple-scattering results here again serve as an idealized experiment against which to test the degree of applicability of single-scattering theory. Also, in the following section the single-scattering FT results are analyzed in detail in order to explain certain discrepancies that will be noted between SCC and MS FT's and also between MS FT's and interplanar distances.

The Fourier transform as carried out in this case can in general be written as

$$F(r)=\frac{1}{2\pi}\int_{k_1}^{k_2}\chi(k)e^{-ikr}g(k)\,dk\ , \qquad (6)$$

where k_1 and k_2 are the upper and lower limits set by the energy window chosen, and $g(k)$ is here selected to be a square window function terminated at nodes in $\chi(k)$. In comparing theory with theory, no inner potential corrections need to be applied here. Both the MS and SSC calculations will also incorporate scattering phase shifts that will depend on θ_j, k, and the specific atom involved. Thus in EXAFS (Refs. 6 and 16) and some prior NPD (Ref. 5) analyses it has been suggested to multiply $\chi(k)$ by a representative $e^{-i[\psi_j(\theta_j,k)+\Phi]}/A_j(k)$ [cf. Eq. (5)] before performing the transform so as to eliminate slight spurious peak shifts; this, however, is not possible in the present case due to the range of scattering angles θ_j that will emerge as being important, and also the way in which the important scattering atoms change with energy. This point is illustrated in Fig. 6, which shows the most important scatterers for several energies as judged according to A_j plotted against scattering angle and path-length difference $r_j(1-\cos\theta_j)$. It is clear that choosing a representative value of A_j or ψ_j at a given k would be very difficult, so we have chosen to Fourier-transform the $\chi(k)$ curves directly. (The same procedure has also been used recently by Tong and Tang[13] in Fourier-transforming multiple-scattering NPD curves.) Finally, we note that the finite k range $\Delta k=k_1-k_2$ used will smear out the Fourier transform in r, perhaps causing an effective averaging over several of the cosine terms in Eq. (5) with very nearly the same path-length differences. As estimates of the Δr values involved, we can use $\Delta k\Delta r\approx 1$ to yield $\Delta r\approx 0.26$ Å over 160—400 eV and $\Delta r\approx 0.14$ Å over 120—590 eV.

Numerical evaluations of Eq. (6) for the curves shown in Fig. 2 are plotted in Fig. 7 as a function of the relevant path-length difference r between a scat-

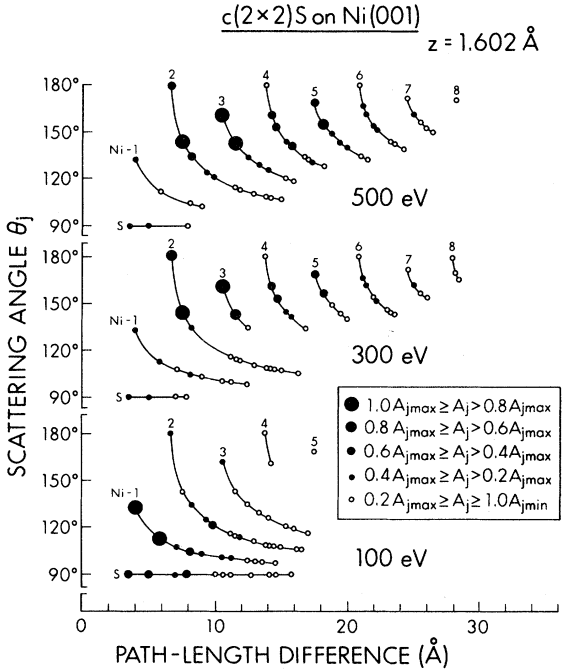

FIG. 6. Plots of the single-scattering angle θ_j against path-length difference for the ~200 strongest scatterers at $z=1.602$ Å and electron energies of 100, 300, and 500 eV. The labels associated with the curves joining the points indicate which layer (S or Ni) the atoms belong to and the size and shading of the points indicate the relative amplitude A_j of the scattered wave (or groups of waves) occurring at a given path-length difference.

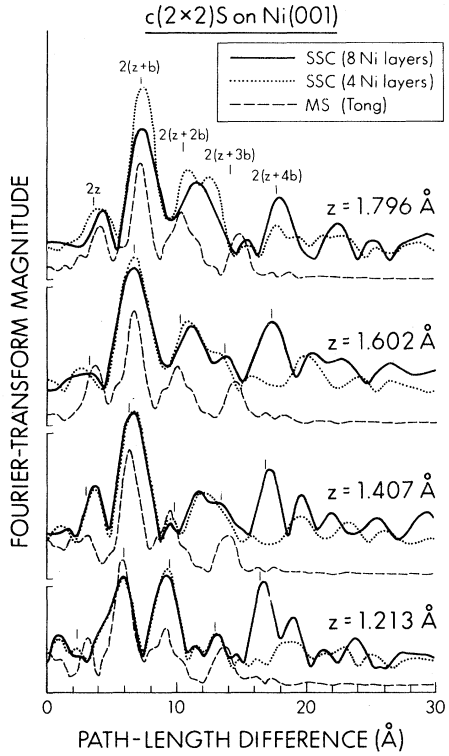

FIG. 7. Fourier transforms of the $\chi(E)$ curves shown in Fig. 2. The perpendicular path-length differences or interplanar distances equal to $2(z+nb)$ from the adsorbate to the first five Ni layers are indicated by tick marks for each z distance. Thus $2z$ corresponds to the first Ni layer, $2(z+b)$ to the second layer, etc.

tered wave and the primary wave, which is expected to be given by $r_j(1-\cos\theta_j)$ in the kinematical formulation [cf. Eq. (5)]. The solid and dotted curves represent the magnitude of the Fourier transform $|F(r)|$ for the eight- and four-layer, unbroadened, single-scattering calculations, respectively, as performed over an $\sim$250-eV energy window from $\sim$160 to $\sim$400 eV. The energy window was chosen to encompass the region of optimum agreement between the results of the kinematical and dynamical calculations, and we have already commented on why the agreement is best over this window. The dashed curves, which have been offset vertically for clarity, but plotted on the same scale, represent the magnitude of the Fourier transform of the multiple-scattering calculations shown in Fig. 2 as taken over an energy window from $\sim$120 to $\sim$590 eV. (The effects of either reducing this range to one comparable with that used for the analysis of the single-scattering data and of expanding the range of the single-scattering analysis to one comparable to the multiple-scattering range will be discussed below.) The tick marks shown in Fig. 7 represent positions corresponding to twice the vertical distances from the adsorbate to the first five substrate layers as determined from the cluster geometry, where b = the Ni interlayer distance = 1.762 Å, and z is a variable absorbate-substrate distance, as indicated on the right-hand side of the figure. Thus $2z$ represents the first Ni layer, $2(z+b)$ the second, etc.

Comparing first the two single-scattering curves given for each z distance, we see that the only large deviations occur for path-length differences $\gtrsim 2(z+4b)$ or $\gtrsim 16$ Å. For example, a prominent peak is present in all of the FT's of the eight-layer results at a distance slightly greater than $2(z+4b)$, which in turn is twice the perpendicular distance from the adsorbate to the fifth Ni layer. However, no such feature is observed in the FT's of the four-layer single-scattering results, *nor* in the corresponding four-layer multiple-scattering FT's. The absence of this fifth-layer feature in the multiple-scattering curves is again evidence of the premature termination of this calculation at the fourth Ni layer. At larger path-length differences the excursions in the magnitude of $F(r)$ are smaller in the FT's of the four-layer single-scattering results than in the FT's of the eight-layer curves. There also exists no correlation between the peak positions of the eight- and four-layer single-scattering curves for $r \gtrsim 16$ Å, since such features must arise from scattering well removed from the backward direction in the four-layer FT's while the equivalent features in the eight-layer FT's can also arise from nearly backscattered waves below the fourth layer. By contrast, at path-length differences less than $2(z+4b)$ the eight- and four-layer single-scattering FT's are in very good agreement as regards both peak positions and amplitudes. There exists, in fact, only one place of significant disagreement and it occurs in the $z = 1.796$-Å curves at $\sim$12 Å where a slight splitting is produced in the four-layer FT while only a single peak exists in the eight-layer FT. Finally, we note that the fifth peak in the eight-layer SSC FT's is a well behaved feature as a function of z distance, occurring at very close to $2(z+4b)$.

The most critical comparison is, of course, between the single-scattering FT's and the corresponding multiple-scattering FT's, which is most self-consistently made using the four-layer single-scattering results. This comparison yields regions of good agreement and other regions of poor agreement. There is generally excellent agreement for both the position and magnitude of the second major peak in the FT's occurring very near a path-length difference of $2(z+b)$. The single-scattering FT for $z = 1.213$ Å probably yields the best overall agreement with its multiple-scattering counterpart as regards peak positions, with the second, third, and fourth peaks of both FT's lying rather close to

one another. This may appear to be a somewhat surprising result since the direct $\chi(E)$ comparison for $z=1.213$ Å of Fig. 2 yields the worst agreement of the four geometries studied. However, a 10-eV shift of the multiple-scattering $\chi(E)$ curve to higher energy produces very good agreement with the single-scattering results over the 160 to 400-eV range, and since the FT is sensitive only to the frequencies of the oscillations but not to the absolute energies at which they occur, the good agreement between the two FT's can be understood.

On the other hand, two distinct kinds of disagreement are found between the single- and multiple-scattering FT's of Fig. 7. The first is the complete absence of structure in the multiple-scattering FT's at distances greater than approximately $2(z+4b)$ as compared with that observed in both the eight- and four-layer FT's over this same range. This lack of structure in the multiple-scattering FT's for path-length differences beyond roughly twice the S-to-fourth Ni layer distance thus *qualitatively* supports the idea of this FT being related to interplanar distances, but we shall see below that this is quantitatively true only for one of the distances involved. The second area of disagreement is the generally poor correspondence between single- and multiple-scattering FT's in the region bounded by the third and fourth peaks in the multiple-scattering FT [i.e., near $2(z+2b)$ and $2(z+3b)$]. Unlike the multiple-scattering curves, the systematic quasilinear behavior of the third and fourth features in the single-scattering FT's as a function of z is poor. Similar discrepancies are also observed for the first peak near $2z$, especially for $z=1.213$ and 1.602 Å. We will later turn to a more detailed explanation of these areas of agreement and disagreement in terms of the exact nature of the scattering atoms most strongly involved.

The effects of a $\pm 3°$ angular broadening on the FT's of the single-scattering results are illustrated in Fig. 8. The curves represent the FT's of the data shown in Fig. 4. The solid curves are the FT's of the unbroadened single-scattering data and the dotted curves the FT's of the broadened data, where the transforms were again performed over the range ~ 160 to ~ 400 eV. The corresponding FT's of the multiple-scattering data from Fig. 7 (dashed curves) are included for comparison. The scales are the same for all curves, but the three sets of curves have been vertically offset for clarity. The effects of angular broadening are most evident in the region between $2(z+2b)$ and $2(z+3b)$ and beyond $2(z+4b)$ for the eight-layer FT's and in the region beyond $2(z+2b)$ for the four-layer FT's. Angular broadening decreases the magnitude of the FT over the entire range shown, with the more pronounced effects

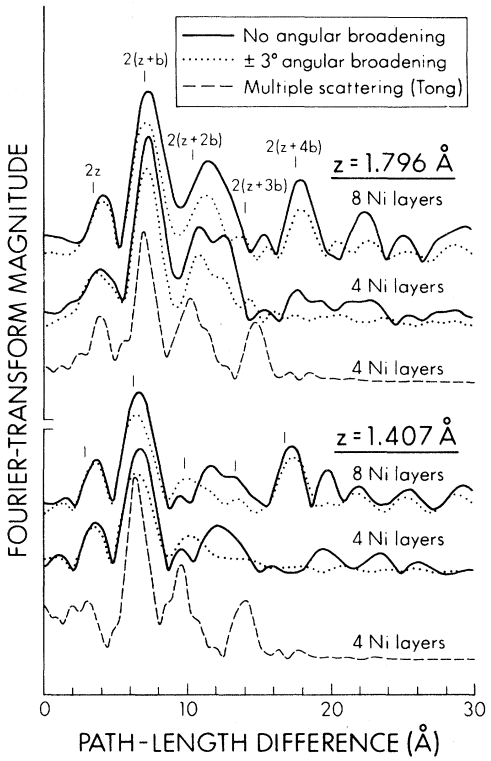

FIG. 8. Fourier transforms of the $\chi(E)$ curves shown in Fig. 4. The perpendicular path-length differences or interplanar distances equal to $2(z+nb)$ from the adsorbate to the first five Ni layers are indicated by tick marks for each z distance.

occurring at distances greater than $2(z+3b)$ in the four-layer transforms. The four-layer FT structure arising from high-frequency oscillations in $\chi(E)$ is almost completely washed out in the dotted curves, in good agreement with the predictions of multiple scattering. The second peak near $2(z+b)$ undergoes a very small shift in position of typically ≤ 0.1 Å, which generally improves the already good agreement with the multiple-scattering FT. Also the agreement in the region of the third peak near $2(z+2b)$ is significantly improved. However, even with broadening there still does not exist a significant feature in the single-scattering FT's that corresponds with the fourth peak in the multiple-scattering FT's near $2(z+3b)$, and there also remains some disagreement between the positions of the first peak near $2z$.

The results of the Fourier-transform analysis are numerically summarized in Table II and schematically illustrated in Fig. 9. Figure 9 compares the FT peak positions with horizontal lines representing path-length differences as based on vertical interlayer distances $2(z+nb)$ for the first five layers ($n=0$, 1, 2, 3, and 4). We begin by considering the average differences in peak positions over all z

TABLE II. Comparison of theoretical NPD Fourier-transform peak positions for $c(2\times2)$S on Ni (001) obtained from single- and multiple-scattering $\chi(E)$ curves. The columns labeled (a) represent FT peak positions from unbroadened $\chi(E)$ curves and those labeled (b) represent peak positions from curves with a $\pm3°$ angular broadening to simulate experimental effects.

SSC-8Ni (Å)		SSC-4Ni (Å)		MS-4Ni (Å)	$2(z+nb)$	SSC-8Ni (Å)		SSC-4Ni (Å)		MS-4Ni (Å)	$2(z+nb)$
(a)	(b)	(a)	(b)	(Tong)	(Å)	(a)	(b)	(a)	(b)	(Tong)	(Å)
		$z=1.213$ Å						$z=1.407$ Å			
				3.20	2.426	3.75	3.60	3.70	3.60		2.814
5.95	6.00	5.90	5.95	5.90	5.950	6.70	6.50	6.75	6.55	6.40	6.338
9.30	9.60	9.30	9.45	9.20	9.474		10.00		10.20	9.60	9.862
13.15		13.10		13.75	12.998					14.05	13.386
16.80	17.10				16.522	17.30	17.45				16.910
		$z=1.602$ Å						$z=1.796$ Å			
				3.70	3.204	4.30	4.25	4.00	3.75	4.10	3.592
6.75	6.85	6.80	6.75	6.70	6.728	7.40	7.25	7.40	7.30	7.15	7.116
11.20	10.95	10.95	10.45	10.00	10.252	11.60	11.50	10.95	10.90	10.40	10.640
13.75	13.75			14.55	13.776					14.85	14.164
17.45	17.90				17.300	18.00	18.10				17.688

values between the broadened and unbroadened single-scattering results, which are 0.14, 0.11, 0.22, and 0.25 Å for the first, second, third, and fifth peaks, respectively. (The fourth peak is not reliably seen in SSC results.) The equivalent average differences between the eight-layer and four-layer peak positions are 0.21, 0.05, and 0.34 Å for the first, second, and third peak positions, respectively. Comparison of the peak positions in the two four-layer SSC FT's with those in the multiple-scattering FT's produces average positional differences of 0.14 and 0.48 Å for the second and third peaks, respectively. (Differences are only quoted for peaks observable in both sets of curves at all four z values.) These numbers substantiate what is observed in Figs. 7 and 8 in that the second SSC peak is found to agree best with its corresponding peak in the FT's of the multiple-scattering curves and in that the position of this peak is least affected by changes in cluster size and angular broadening. Turning now to the average displacement Δd of a given peak in the FT of the single-scattering results from twice the perpendicular interlayer distances, we find that this is 0.67 Å for the first peak. The multiple-scattering curves yield a corresponding value for the first peak of $\Delta d=0.59$ Å. The second peak gives Δd values of 0.15 and 0.04 Å from the single- and multiple-scattering FT's, respectively. The third and (sometimes very weak) fourth peaks give Δd values of 0.43 and 0.07 Å for the single-scattering FT's and 0.26 and 0.72 Å for the multiple-scattering FT's, respectively. The single-scattering Δd for the fifth peak near $2(z+4b)$ is 0.41 Å. Thus it is only for the second peak that the vertical interplanar path-length difference $2(z+b)$ is found in both single- and multiple-scattering FT's with high enough accuracy that it might be considered directly useful in a structural sense. [Even for this second-layer peak, we will in the next section show that the agreement with $2(z+b)$ is fortuitous.] For all other peaks the Δd values are ~0.25–0.7 Å in magnitude for both single- and multiple-scattering peaks.

At this point, it is also necessary to consider the effects on the FT's of changing the energy range to be transformed, as this is a somewhat arbitrary choice usually dictated by the range of theory or experiment available. Changing the range of the multiple-scattering FT's to a smaller one comparable with that of the single-scattering analysis shifts the second peak by typically 0.15 Å to lower values and so has little effect on the good agreement in this region; such a shift is rather large in comparison to the structural accuracy that might be desired from such an NPD analysis, however. Also, the multiple-scattering FT's over the smaller range do exhibit significant changes in the positions of the first, third, and fourth peaks. These peaks are no longer as well behaved, as they vary in position somewhat randomly as a function of z. The third and fourth peaks, in fact, behave in a fashion similar to that observed for the corresponding peaks in the single-scattering FT's; hence the agreement between the third peak positions and $2(z+2b)$ is worsened while the agreement between the fourth peak positions and $2(z+3b)$ is improved. The agreement between the first peak position and $2z$ is also im-

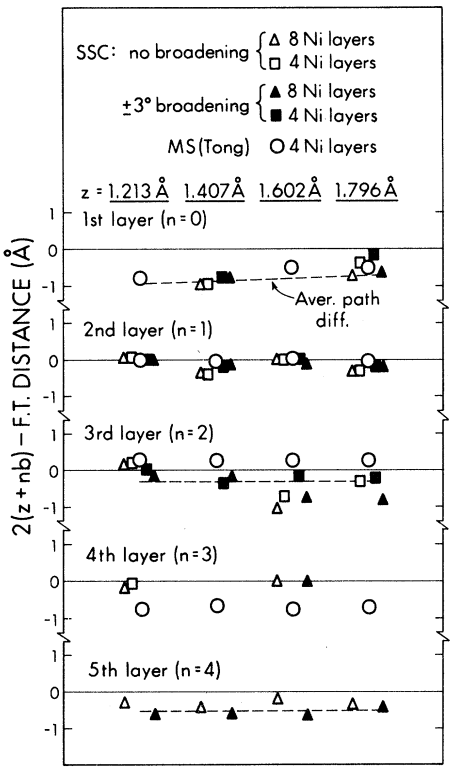

FIG. 9. Peak positions in the Fourier transforms of both the single- and multiple-scattering $\chi(E)$ curves are plotted with respect to the perpendicular path-length differences or interplanar distances equal to $2(z+nb)$ from the adsorbate to the first five Ni layers, which are shown as horizontal solid lines. The dashed lines indicate peak positions estimated from an analysis of the single-scattering formalism and are based upon an average path-length difference for the most dominant scatters [see Eq. (5)].

proved, but the Δd value here is already so large that this has little structural significance. Thus the full energy range seems necessary in the multiple-scattering FT's to yield a series of peaks with linear behavior in z, but the peak where best agreement is obtained between path-length difference and twice the interplanar distance is the least affected.

Conversely, we also have investigated the effects of expanding the FT energy range for the single-scattering curves. Two extensions were made to the range of the single-scattering FT's shown in Figs. 7 and 8. The first involved extending the range at the high-energy cutoff out to ~ 580 eV while the low-energy cutoff remained unchanged at ~ 160 eV. The second involved extending the entire range to a value comparable with that used in the multiple-scattering FT's (i.e., ~ 110 to ~ 580 eV), although this to be sure includes energies too low to expect single scattering to be an adequate description (cf. Fig. 2). Both changes introduced more fine structure in the magnitude of the FT's. Below $\sim 2(z+4b)$ the FT's were essentially equivalent for both the broadened and unbroadened eight- and four-layer curves. In the FT's of the broadened eight-layer results over the range ~ 160 to ~ 580 eV the second peak was uniformly shifted in position by 0.15 Å toward larger values with respect to the corresponding values in Table II. The linearity of the third peak as a function of z was significantly improved, along with its position relative to the $2(z+2b)$ values ($\Delta d = 0.11$ Å). The positions of the fifth peak near $2(z+4b)$ remained unchanged with respect to the corresponding values in Table II. However, there was still no indication of a reliable fourth-layer peak near $2(z+3b)$ and the behavior of the first peak remained unpredictable despite the larger range. The same analysis for the unbroadened eight-layer data produced the same effect on the second peak (i.e., a 0.15-Å shift). However, the third-layer peaks were again found to be unreliable, as they were masked by additional structure, and the fifth-layer peaks were uniformly shifted by 0.3 Å to larger values. The behavior of the first-layer peak remained unchanged and again there was no evidence of a fourth-layer peak near $2(z+3b)$. Extending the FT range one step further to $\sim 110 \rightarrow \sim 580$ eV produced significant changes to the positions of the second-layer peak (typically 0.5 Å with respect to the values in Table II) in both the broadened and unbroadened eight-layer data. However, the positions and behavior of the other peaks were essentially unchanged from that described for the $\sim 160 \rightarrow \sim 580$ eV FT's. Thus we conclude overall that the energy range of the Fourier transform in either the multiple- or single-scattering cases is a critical parameter if one is interested in peak positions with a reliability of better than $\sim \pm 0.1$ Å. However, it is significant that the general behavior of the different peaks as a function of z (as e.g., the second and fifth peaks in single-scattering FT's) does not change appreciably with a change in transform range. In what follows, we will thus continue to use our prior choices of ~ 160—400 eV (the region of best agreement between SSC and MS) for single-scattering FT's and ~ 120—590 eV for multiple-scattering FT's.

D. Analysis of the Fourier-transform results

Returning again to the initial FT comparisons in Figs. 7 and 8, there arise several questions that it is of interest to try to answer by a more detailed analysis of the single-scattering model. For example, why is it that the third- and fourth-layer peaks in the SSC FT's do not show a good correlation with

the vertical interplanar path-length differences $2(z+2b)$ and $2(z+3b)$, nor with the FT's of the multiple-scattering results? Also, why do these SSC peaks not show any easily predictable motion as a function of z by contrast to the rather exact interlayer distance tracking of the second-layer peak near $2(z+b)$ and the very linear behavior of the fifth-layer peak near $2(z+4b)$? Also of considerable concern in the multiple-scattering FT's are the rather large discrepancies between the positions of the first-, third-, and fourth-layer peaks and their respective $2(z+nb)$ values (cf. Fig. 9). The following analysis suggests that the answers to all of these questions can be provided by considering the most important scatterers as judged by the SSC model and then noting both the path-length differences $r_j(1-\cos\theta_j)$ and the relative overall phase differences $kr_j(1-\cos\theta_j)+\psi_j+\Phi$ between scattered waves from different atoms or groups of atoms within the same layer. The path-length difference largely determines where a peak will occur in a single-scattering FT and the relative overall phase difference will determine how two sinusoidal terms will add over the transform region.

Fortunately, the simplicity of the single-scattering model permits easily isolating which atomic scattering events ought to be the most important in producing these peaks and thus better understanding the behavior of all of the FT's. That is, Eq. (5) shows that NPD FT's should produce peaks in $|F(r)|$ at distances r equal to the path-length differences $r_j(1-\cos\theta_j)$ and with heights proportional to the A_j's (cf. Fig. 6). (For the moment, we neglect additional effects due to possible near-destructive interferences of different sinusoidal terms in Eq. (5) involving very nearly the same path-length difference, but these will be considered later.) As a first illustration of this, for the odd-numbered Ni layers for which no Ni atom lies directly under a fourfold S atom (cf. Fig. 1), peaks in $|F(r)|$ will then be expected to occur at distances greater than $2(z+nb)$ because $r_j > z+nb$ and $\theta_j < 180°$. The most important path-length differences associated with the first and third layers involve the four nearest-neighbor atoms to the backscattering direction and these are shown plotted as dashed lines relative to $2(z+nb)$ values in Fig. 9. For the fifth layer, four *next*-nearest neighbors are also important enough to be included in the path-length difference estimate via a weighted sum. In general, the FT peak positions of the first, third, and fifth layers agree better with these path differences than with $2(z+nb)$. One finds that the first-layer multiple-scattering peaks lie very much closer to this most important path-length difference ($\Delta d = 0.21$ Å) than to $2z$, as do the majority of the first-peak distances in the single-scattering FT's ($\Delta d = 0.15$ Å). Hence the earlier disagreement with the $2z$ values is rather simply explained by using the evidently more correct path-length differences of the scattered waves. Similarly, the FT peak positions from the single-scattering curves for the third and fifth layers are in better agreement with path-length differences than $2(z+nb)$ distances, having Δd values of 0.33 and 0.15 Å, respectively, when measured with respect to the most important path-length difference. The only exception to this simple analysis is that the third-layer peak in the multiple-scattering FT's is shifted slightly in the opposite direction to that expected on the basis of path-length difference. Thus the use of a most important path-length difference serves to further explain most of the systematics of Fig. 9, but a more detailed dissection of the single-scattering results is needed to go further. As a final qualitative comment, we note that the very large disagreement between $2(z+3b)$ and the fourth-peak position in the multiple-scattering FT's is not surprising in view of the absence of a fourth-layer peak in the majority of the single-scattering FT's; this is explained below.

It is useful now to select out only those atoms that contribute most significantly to the NPD oscillations. Thus the ~ 200 strongest scatterers were chosen from the large eight-layer cluster at various energies and for all z positions on the basis of their A_j values, where A_j is defined below Eq. (2). The important information associated with these ~ 200 strongest scatterers is summarized in Fig. 6 for $z = 1.602$ Å and energies of 100, 300, and 500 eV. Essentially equivalent results were obtained for the other z positions. The dot size and shading represent the strength of the scattered wave (or waves) from an atom (or a group of atoms) with a given path-length difference. Their scattering angles have been plotted as a function of their path-length difference. The dots have been joined by lines to group those atoms that belong to the same layer and the layers have been labeled at the top of each line (S represents sulfur, 1 represents the first Ni layer, etc.). The same absolute number of atoms (~ 200) is plotted for each energy, although at larger scattering angles the degeneracy N_j within the dots (that is, the actual number of atoms which by symmetry have the same r_j and θ_j) increases, resulting in what superficially looks like a smaller total number of atoms at 100 eV. The relative amplitudes are correct at a particular energy but have been arbitrarily scaled to $A_{j\max}$ for each of the energies shown and A_j here allows for summing over symmetry degeneracy in r_j and θ_j.

The effects of the peak in the backscattering amplitude over the range ~ 160 to ~ 400 eV (cf. Fig. 3)

are evident in the distribution of atoms as a function of energy. At lower energies of ~ 100 eV, strong scattering is confined to the near-neighbor atoms, with no strong directional dependence evident since $|f(180°)|$ is more comparable in amplitude to all other scattering directions. Also at 100 eV, one notices the penetration cutoff due to Λ_e, as very little significant scattering occurs below the third Ni layer. At 300 eV, the peak in $|f(180°)|$ produces strong directional dependence in the scattering, with the strongest scatterers found close to the backward direction. Also, even at this intermediate energy some significant scattering occurs in the sixth and seventh layers. At higher energies of ~ 500 eV, the effects of a decreasing $|f(180°)|$ begin to emerge again, with the strongest scatterers moving away from the backward direction. Also at higher energies, the increased penetration due to a larger Λ_e is apparent, with important atoms for scattering existing out to the eighth layer.

It should be noted that for Ni (001) up to eight atoms can contribute to the strength of the scattering at certain path-length differences rather near the $2(z+nb)$ values. One example of this summation of amplitudes is illustrated in the second Ni layer at 300 eV, where the backscattered wave amplitude from the single Ni atom directly below a S atom is less than the sum of intensities from its four nearest-neighbor atoms in the same plane, despite the fact that the amplitude of its scattering factor at 180° $|f(180°)|$ is nearly four times greater than the amplitude of the scattering factor associated with the nearest-neighbor scattering $|f(\sim 140°)|$. In general, the degeneracy of the atoms for a particular path-length difference in Ni (001) as counted outward from the backscattering direction goes as 1,4,4 for even-numbered layers and as 4,8 for odd-numbered layers. One would expect then that the peaks in the FT's will occur at distances corresponding to some weighted average of the path-length differences for the strongest few scatterers within each layer. Hence the FT peaks should occur at distances slightly greater than $2(z+nb)$ for each and every layer *unless* additional interference effects from the layers directly above are important.

To examine this further, Fig. 10 shows the A_j values of the strongest ~ 200 scatterers (obtained at an energy of 220 eV) in the form of a bar plot superimposed on the FT's of the eight-layer unbroadened single-scattering results. The two strongest sets of scatterers in each layer are labeled with their respective layer numbers down to the fifth layer. Inspection of this figure shows that the FT peaks associated with the second, fifth, and to a lesser degree also the first and third, Ni layers occur rather close to the position of a weighted average of the path-length

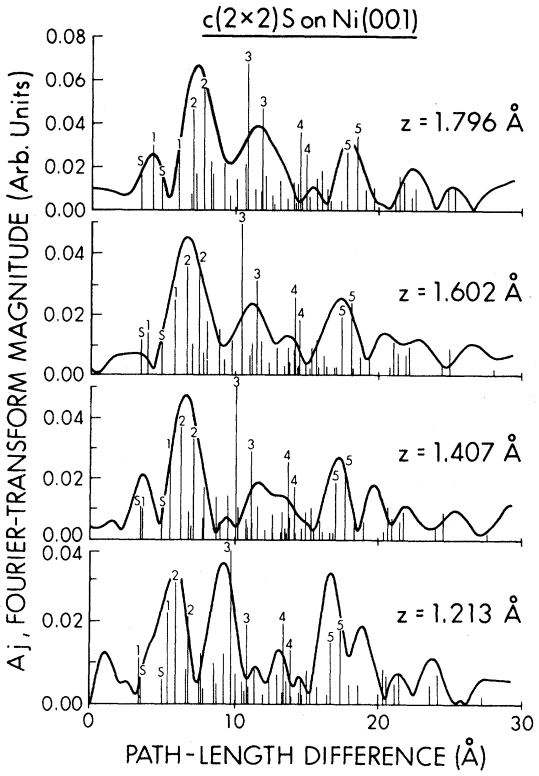

FIG. 10. Fourier transforms of the single-scattering $\chi(E)$ curves obtained with an eight-layer atomic cluster and no angular broadening (solid curves in Fig. 2). Superimposed on these curves are vertical bars proportional in length to the A_j values of the strongest ~ 200 scatterers obtained at an electron energy of 220 eV. The labels associated with the dominant A_j values represent the atom and layer from which the scattering originates (S represents sulfur, 1 represents the first Ni layer, 2 represents the second Ni layer, etc.).

differences of the strongest scatterers in that layer. However, there are also some significant discrepancies with respect to this simple viewpoint, for example, in that the largest peak in the FT's does not always correspond to the largest A_j value. That is, the relative magnitude of $F(r)$ in the region of both the third and fourth layers is much smaller than what one would expect on the basis of the corresponding A_j values, whereas the positions and relative strengths of the second- and fifth-layer features appear to be correctly predicted by their corresponding A_j values. The reason for this seemingly anomalous behavior in the third and fourth layers (which also show the greatest discrepancies between SSC and MS curves) lies in the fact that a relative overall phase shift is introduced between the two dominant types of scatterers within a layer. A simple geometrical analysis which also includes the phase shifts

ψ_j introduced by scattering shows that the relative overall phase shift between the two third-layer peaks in the bar plot for $z=1.213$ Å varies from 100° to 270° over the FT energy range of ~ 160 to ~ 400 eV. The corresponding relative phase shifts for $z=1.407$, 1.602, and 1.796 Å are 90°—250°, 80°—230°, and 70°—220°, respectively. Thus the two third-layer peaks will be nearly 180° out of phase with each other over a major portion of the FT range. This phase difference is in turn responsible for the relatively low value of $|F(r)|$ in this region and the poorly behaved character of this feature as a function of z. Applying the same analysis to the two dominant fourth-layer peaks in the bar plots produces relative phase shifts between the two of 170°—250°, 165°—245°, 160°—240°, and 160°—235° for the same four z values over the FT range. These phase shifts bracket 180° even more closely, and thus these two fourth-layer peaks will essentially negate one another over this range, thereby explaining why a corresponding fourth-layer peak is not observed in the majority of the single-scattering FT's. (Such cancellations of two close-lying sinusoidal terms have also been noted in EXAFS, for example, near the Ti edge in a Cu_2Ti alloy by Raoux *et al.*[17]) The much more well-behaved fourth-layer peak found in the multiple-scattering FT's appears to be a direct result of the larger energy range transformed. Here the FT's are picking up the oscillations from the fourth layer at energies above 400 eV where the two fourth-layer A_j peaks are no longer $\sim 180°$ out of phase. However, at these energies the fourth-layer atom directly underneath the emitter is no longer a relatively strong scatterer compared to the summed scattered wave amplitudes from other atoms in this layer. This is illustrated in the 500 eV data of Fig. 6, where the first two fourth-layer path-length differences greater than $2(z+3b)$ produce the strongest scattering. Hence one would expect the fourth-layer peak in the FT to be approximately halfway between these two A_j values or, in terms of the perpendicular distance, 0.68, 0.66, 0.64, and 0.63 Å greater than $2(z+3b)$ for $z=1.213$, 1.407, 1.602, and 1.796 Å, respectively. The fourth-layer peak distances from the multiple-scattering FT's are in fact found at 0.75, 0.67, 0.67, and 0.69 Å greater than $2(z+3b)$ for $z=1.213$, 1.407, 1.602, and 1.796 Å, respectively, in excellent agreement with the distances predicted by the above analysis.

The features in the FT curves of Fig. 10 which generally correspond to a set of high A_j values can also be self-consistently explained by this simple model. The second- and fifth-layer FT peaks from the single-scattering data are well behaved for reasons essentially opposite to those given to explain the behavior of the third- and fourth-layer peaks. In the case of the fifth-layer peak, the two A_j peaks in the bar plots are found to be in phase with one another over a major portion of the FT range. The fifth-layer peak in the FT should occur then approximately halfway between these two path-length differences, as their scattered-wave amplitudes are approximately equal; this position is indicated by the dashed line in Fig. 9. This more straightforward behavior also then permits predicting that Fourier transforms of a multiple-scattering calculation including five or more Ni layers *or* broad-range experimental data would show a very strong fifth-layer peak. Unlike the other peaks discussed up to this point, the second-layer peak is produced by three closely grouped A_j components, one originating from the first Ni layer and the other two from the second Ni layer, as illustrated in Fig. 10. Again, geometrical analysis shows that the two second-layer contributions are essentially in phase with one another over the range of the FT with this phase coherence being responsible for the well behaved character of the second-layer peak as a function of z. The contribution of the first-layer atom to this second-layer peak is somewhat more difficult to characterize because its relative phase and amplitude with respect to the second-layer components vary rapidly with z and electron energy, respectively. The z distance of 1.407 Å is the only z where the first-layer component is out of phase with respect to the component from the second-layer Ni atom directly underneath the emitter over the major part of the FT range. The first-layer component varies from nearly in phase to out of phase over the FT range for the other z distances. Expanding the FT range shifts the position of this second-layer peak in the single-scattering FT's in a fashion totally consistent with an analogous analysis of A_j's and path-length differences, whereas the position of this same peak in multiple-scattering FT's is insensitive to changes in the FT range. Probably this insensitivity is some consequence of multiple-scattering effects.

This analysis of Fig. 10 and its relationship to both single- *and* multiple-scattering FT's thus clearly illustrates that Fourier-transform analyses of NPD spectra produce features in $|F(r)|$ that are most directly related to the path-length differences involved and not to perpendicular interlayer distances. A further important point is that some peaks in $|F(r)|$ shift by as much as 0.9 Å when the Fourier-transform range is changed from ~ 250 to ~ 450 eV for both single- *and* multiple-scattering curves. Thus the overall accuracy of the Fourier-transform method in NPD is questionable. This sensitivity to the transform range is especially strong for peaks in which destructive interferences may occur between scattered waves originating in the same

layer. Furthermore, any attempt to minimize the disagreement between the peak positions in $|F(r)|$ and the $2(z+nb)$ distances by adjustment of the inner potential[5] is physically unsound and probably will produce only artificial estimates of the accuracy of this method for structural analysis. And the more recent suggestion by Tong and Tang[13] of theoretically deriving empirical shifts between FT peaks and $2(z+nb)$ values for later use in structural determinations of experimental data thus also seems dubious in view of the possible sensitivity of such shifts to both the FT range *and* the particular adsorbate geometry involved.

Finally, this type of single-scattering analysis could be extended to any number of adsorption systems provided that the behavior of the scattering factors for the substrate and adsorbate are known as a function of energy. Then a simple geometric calculation including scattering phase shifts would permit determining which peaks in the FT should be least affected and which most affected by changes in the FT range. The more reliable structural information will obviously come from those peaks that are relatively insensitive to changes in the energy range.

IV. CONCLUSIONS

Extensive comparisons have been made between NPD results as derived from both single-scattering cluster calculations and multiple-scattering calculations[13] for $c(2\times2)$S on Ni (001) over the electron kinetic energy range from 100 to 600 eV. It is found that the SSC model gives a good description of the NPD $\chi(E)$ curves as obtained from MS calculations over the energy range 160—400 eV, whereas the agreement is found to be poor for energies outside this range. The amplitude of the scattering factor is shown to be peaked in the backward direction over this same energy range and this behavior in $|f(180°)|$ qualitatively explains the regimes of agreement and disagreement observed between the results of the two calculations as a function of energy. It is thus suggested that extending the energy range in experimental NPD spectra (or in fact, also in EXAFS measurements) to higher energies need not result in any theoretical simplifications, but in fact, may add further complications in terms of the need for larger atomic clusters, more partial-wave phase shifts, and a greater influence of multiple-scattering effects.

It was shown that increasing the single-scattering cluster size from one that contained four Ni layers to one that contained eight Ni layers had significant effects on the predicted NPD curves, particularly at energies greater than 300 eV. However, the multiple-scattering NPD data that have been published to date have been terminated at the fourth Ni layer and so may well be in error at energies greater than 300 eV.

The inclusion of a $\pm3°$ instrumental angular broadening in the single-scattering calculations was found to decrease the amplitude of the oscillations over the entire energy range and to shift peak positions in some instances by as much as 10 eV. The agreement between the results of broadened eight-layer single-scattering calculations at $z=1.35$ Å and experimental NPD data for $c(2\times2)$S on Ni (001) (Ref. 9) was also found to be very good over the energy range ~170 to ~430 eV, and in fact was better than that for multiple-scattering calculations[10,13] for higher energies of ~300—430 eV. However, the degree of discrepancy that does exist between single scattering and experiment over the 170—430-eV energy range probably precludes the use of a simple kinematical model for highly accurate structural analysis; nonetheless, it is reasonable to propose that the kinematical curves could be used to distinguish between different types of adsorption site (e.g., atop, bridge, fourfold hollow) as a first step in analyzing NPD data.

It has been clearly demonstrated that a Fourier-transform analysis of single- and multiple-scattering $\chi(E)$ curves produces peaks in the magnitude of the Fourier transform at distances most directly related to the relevant path-length differences involved and *not* to the perpendicular adsorbate-to-substrate interlayer distances. Although the FT's of both multiple- and single-scattering NPD curves agree very well for the second-layer peak occurring near $2(z+b)$, this peak is found to involve both first- *and* second-layer scattering strongly and only to fortuitously lie so close to an interplanar distance. Also, the peak positions have been found to be sensitive to the energy range of the Fourier transform, thus adding further uncertainty to this type of analysis. It thus remains to be seen whether the empirical reliability of this second-layer peak and hence the accuracy of the FT technique are a result of a particular fortuitous choice of geometry or whether this peak indeed is a feature one can use in general to obtain accurate structural information from no matter what the type of adsorption site or crystal structure. At this point it is evident that great care needs to be exercised when employing Fourier-transform analyses of NPD data. Finally, we stress that NPD is primarily sensitive to changes in the path-length differences of various scatterers and thus only indirectly sensitive to perpendicular interlayer distances.

ACKNOWLEDGMENTS

We are very much indebted to S. Y. Tong for providing us with multiple-scattering curves prior to publication and to D. A. Shirley for making experimental data available to us prior to publication. This work was supported by National Science Foundation Grant No. CHE80-21355.

[1]S. D. Kevan, D. H. Rosenblatt, D. R. Denley, B.-C. Lu, and D. A. Shirley, Phys. Rev. Lett. 41, 1565 (1978).
[2]C. H. Li and S. Y. Tong, Phys. Rev. Lett. 43, 526 (1979).
[3]D. H. Rosenblatt, J. G. Tobin, M. G. Mason, R. F. Davis, S. D. Kevan, D. A. Shirley, C. H. Li, and S. Y. Tong, Phys. Rev. B 23, 3828 (1981).
[4]D. H. Rosenblatt, S. D. Kevan, J. G. Tobin, R. F. Davis, M. G. Mason, D. R. Denley, D. A. Shirley, Y. Huang, and S. Y. Tong, Phys. Rev. B 26, 1812 (1982).
[5]Z. Hussain, D. A. Shirley, C. H. Li, and S. Y. Tong, Proc. Natl. Acad. Sci. U.S.A. 78, 5293 (1981).
[6]D. E. Sayers, E. H. Stern, and F. W. Lytle, Phys. Rev. Lett. 27, 1204 (1971); Phys. Rev. B 11, 4836 (1975).
[7]J. E. Demuth, D. W. Jepsen, and P. M. Marcus, Phys. Rev. Lett. 31, 540 (1973).
[8]S. Brennan, J. Stöhr, and R. Jaeger, Phys. Rev. B 24, 4871 (1981).
[9]Z. Hussain and D. A. Shirley (private communication).
[10]S. Y. Tong (private communication).
[11]S. Kono, S. M. Goldberg, N. F. T. Hall, and C. S. Fadley, Phys. Rev. B 22, 6085 (1980), and earlier references therein.
[12]P. J. Orders, R. E. Connelly, N. F. T. Hall, and C. S. Fadley, Phys. Rev. B 24, 6163 (1981).
[13]S. Y. Tong and J. C. Tang, Phys. Rev. B 25, 6526 (1982).
[14]M. P. Seah and W. A. Dench, Surf. Int. Anal. 1, 2 (1979).
[15]S. D. Kevan, Ph.D. thesis, University of California, Berkeley, 1980 (unpublished).
[16]P. A. Lee and G. Beni, Phys. Rev. B 15, 2862 (1977).
[17]D. Raoux, J. F. Sadoc, P. Lagarde, A. Sadoc, and A. Fontaine, J. Phys. (Paris), Colloq. 41, C8-207 (1980).